JOURNAL OF MATERIALS SCIENCE 19 (1984) 4061–4067

Measurement of thin-layer surface stresses by indentation fracture

BRIAN R. LAWN, EDWIN R. FULLER, Jr
Center for Materials Science, National Bureau of Standards, Washington, DC 20234, USA

A model is developed for evaluating stresses in the surfaces of brittle materials from changes in indentation crack dimensions. The underlying basis of the model is a stress intensity formulation incorporating the solution for a penny-like crack system subjected to a constant stress over a relatively thin surface layer. Results from a previous study of surface damage in proton-irradiated glass are used to illustrate the scope of the method. The indentation fracture analysis also provides some fresh insight into the susceptibility of brittle surfaces to spontaneous cracking. Implications of the study concerning the potential effect of surface stresses on mechanical properties, such as strength, erosion and wear, are briefly discussed.

1. Introduction

Surfaces of solids can exist in a state of residual stress. There is a diversity of ways in which surface stresses may arise; mechanical finishing (machining, etc.), thermal tempering, chemical treatment, radiation damage. These stresses can attain unusually high intensities, even if only over a shallow layer beneath the surface. Accordingly, surface history can be an important factor in the consideration of mechanical properties of materials, such as strength and erosion.

It is not generally an easy matter to measure surface stresses. Traditional methods, e.g. X-ray diffraction line shifts, deflection of thin substrates, optical birefringence, require a good deal of special expertise and are limited in the material configurations to which they can be applied. A relatively new and simple approach in the case of inherently *brittle* materials is to introduce indentation cracks into the test surfaces [1–3]. The surface traces of the cracks extend or contract, depending on whether the residual stresses are tensile or compressive, so development of a stress layer may be followed systematically by monitoring the crack size. However, detailed fracture mechanics analyses have thus far been limited to "deep-layer" configurations, where the stresses extend to a sufficient depth below the surface that they may be considered as uniform over the crack area [3]. Most practical cases do not conform to the spirit of this approximation, so the indentation technique has been severely restricted in its application.

In this work we redress this shortcoming by extending the fracture mechanics analysis to "thin-layer" stress configurations. We focus particular attention on the case where the depth of the layer is small compared to that of the crack, assuming once more that the stresses remain uniform within this layer. However, the formalism used to obtain the solution for this configuration may be carried over to more general layer stress distributions. Indentation fracture data from an earlier study on photon-irradiated glass surfaces [1] will be used to illustrate the quantitative information that may be obtained from the analysis.

2. Fracture mechanics model

Consider the crack pattern produced by a standard "point" indenter [4], e.g. Vickers, Knoop. Basically the cracks have penny-like geometries, with their centres at or close to the point of contact. There are two main types of cracks: *radial/median* (hereafter referred to simply as radial), on symmetry planes normal to the surface and containing the load axis [5, 6]; *lateral*, on shallow subsurface planes approximately normal to the load axis [7]. Of these two systems it is the first which is of

0022–2461/84 $03.00 + .12

greater interest here, for the main components of surface stress fields are laterally directed. Thus the radial crack traces on the specimen surface should constitute a sensitive indicator of induced stress levels.

We begin by reviewing the fracture relations for radial cracks in the absence of any surface stresses, in order to establish a reference base. It is supposed that the crack system is sufficiently well developed that the radial arms extend well beyond the hardness impression from which they emanate, but not too large that lateral chipping disrupts the pattern. Experimentally, this means operating within a specifiable range of contact loads. A key element in the fracture evolution is the stable growth of the radial segments on *unloading* the indenter, indicating that the primary crack driving force arises from the irreversible component of the elastic–plastic contact field [5]. Consequently, the immediate post-indentation surface radial configuration is subject to a *residual* stress intensity factor [5, 6]

$$K_r = \chi P/c^{3/2} \quad (1)$$

where P is the peak contact load, c is the characteristic crack size, and χ is a dimensionless factor which represents the intensity of the persistent field (Fig. 1). One manifestation of this residual driving force is the continued crack growth observed well after completion of the indentation cycle in non-equilibrium fracture conditions [5, 8].

Now suppose the radial crack system is acted upon by surface stresses, Fig. 1. The essence of our approach here is to take the fracture mechanics solutions for a concentrated force acting on an elemental area within the crack perimeter [9] and to integrate this solution over the entire crack area. In principle, this procedure could be used to obtain a general stress intensity factor for any depth profile of stress. Details of such calculations are included in the Appendix. For simplicity, we restrict our present attention to the special case of a stress σ_s distributed uniformly over a depth $d \ll c$ (thin-layer approximation). This approximation is tantamount to regarding the stress system as a surface line force, $\sigma_s d$. The appropriate stress intensity factor at the specimen surface for this case is

$$K_s = 2\psi\sigma_s d^{1/2} \quad (2)$$

where ψ is a crack geometry term of value about unity. Implicit in any such calculation of this kind is the assumption that the crack remains penny-like in its geometry. In reality, the opening or closure of the radial arms will be accentuated in the vicinity of the stress layer, in which event Equation 2 is subject to some uncertainty. It may be noted that, within the bounds of our approximation, the stress intensity factor in Equation 2 is independent of crack size. Compensatory effects are in evidence here; the extent of the stress layer sampled by a larger crack is greater in *absolute* terms, but smaller in *relative* terms (i.e. in comparison to the total crack area).

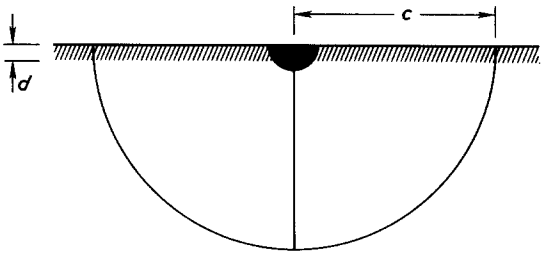

Figure 1 Schematic showing mutually orthogonal radial crack system produced by Vickers indentation and subjected to surface stress. Cracks have penny-like geometry centred about central deformation zone (dark region), which provides residual driving force. Layer depth d over which stress σ_s acts (shaded) is assumed to be small in comparison with radial crack dimension c.

Provided the surface stress layer does not alter the characteristics of the elastic–plastic properties embodied in the χ term of Equation 1, we may use the principle of superposition to obtain the total stress intensity factor for the radial crack system. Hence, adding Equations 1 and 2 we have

$$K = \chi P/c^{3/2} + 2\psi\sigma_s d^{1/2} \quad (3)$$

evaluated at the specimen surface. For equilibrium fracture conditions the cracks extend when K reaches a critical value, K_c (toughness). Equation 3 may then be rewritten in the form

$$\chi P/c^{3/2} = K_c - 2\psi\sigma_s d^{1/2} \quad (4)$$

Note that the imposition of the surface stress is equivalent to reducing or increasing the intrinsic resistance to fracture, depending on whether σ_s is tensile or compressive, respectively. In the former instance there is an interesting limit to σ_s, whereby the "effective toughness" on the right-hand side is reduced to zero; at this point the crack size becomes infinite, corresponding to unlimited, spontaneous extension of the radial cracks across the specimen surface. A slightly more convenient form for our expression may be obtained by using

the reference state of zero surface stress to eliminate χ; thus, inserting $c = c_0$ at $\sigma_s = 0$ into Equation 4, we have finally

$$2\psi\sigma_s d^{1/2}/K_c = 1 - (c_0/c)^{3/2} \quad (5)$$

Stress evaluation is thereby reduced to a measurement of relative crack dimensions in the stressed and non-stressed states.

3. Case study: proton-irradiated glass

As an illustration of the utility of the above fracture mechanics model we consider some results from a study of radiation damage in soda-lime silicate glass [1, 10]. In this study float glass surfaces were bombarded with protons under an accelerating voltage of 480 kV, and the resulting stresses were evaluated using Vickers indentations. Exhaustive surface stress measurements had previously been made by Eernisse on similar glass surfaces (fused silica) for a variety of ion sources, including protons, using a sensitive bar deflection technique [11]. Eernisse found the induced stress to be tensile, and to increase linearly with radiation dose up to a saturation level, beyond which the level tended to fall off. For high energy protons this saturation occurred at a dose somewhat in excess of 10^{19} ions m^{-2}, at which the critical surface force was $\sigma_s d \simeq 500\,N\,m^{-1}$ [11]. This critical force was in fact found to be the same for all radiation treatments studied, independent of ion type or energy, indicating that the saturation phenomenon reflected some property of the glass surface. Eernisse was unable to identify the true nature of this property.

In our experiments indentation crack size was monitored for doses up to 10^{21} protons m^{-2} [10]. A fixed load of $P = 5.9\,N$ was used for all tests. At this load the crack patterns were always well developed in the sense indicated earlier (Section 2). For the glass surface in the unirradiated state the surface radial crack size was $c_0 = 63\,\mu m$, well in excess of the penetration depth $d = 5\,\mu m$ expected for 480 kV protons [11], in conformity with the thin-layer approximation embodied in Equation 2. Unfortunately, the indentations were made in air so some post-contact crack growth must have occurred, in which case the c values reported here do not represent true equilibrium configurations. Nevertheless, since Equation 5 is formulated in terms of *relative* crack sizes we can argue that we should at least be able to follow data *trends*. Unlike the dimensions of the radial cracks, the dimensions of the hardness impressions were relatively insensitive to the radiation treatment [1], suggesting that the residual contact term χ in Equation 3 may indeed be regarded as an invariant quantity.

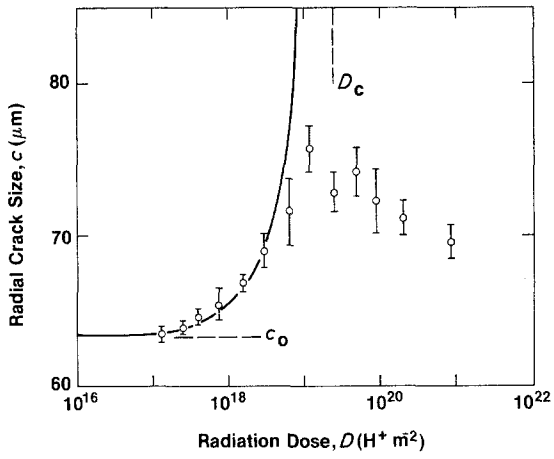

Figure 2 Radial crack size for indentations ($P = 5.9$ N) in soda-lime glass as function of proton radiation (480 kV) dose. Curve through data points is fit to Equation 7 using c_0 and D_c values indicated.

The results of the crack-size measurements are plotted as a function of ion dose in Fig. 2. The data points represent means and standard deviations for at least eight indentations at each dose level. The initial rise of the c values indicates development of a tensile stress, and the subsequent fall-off a saturation limit, consistent with the findings of Eernisse. During the course of the routine crack measurements the explanation of this saturation became clear [10]. At doses around 1×10^{19} protons m^{-2} the glass surfaces showed signs of incipient "crazing" around the indentations (where high residual contact stresses persist). At slightly higher doses, 2 to 3×10^{19} protons m^{-2}, the surfaces crazed spontaneously, presumably from pre-present (or perhaps even radiation-induced) surface "flaws" [12, 13]. An example of such spontaneous cracking is shown in Fig. 3. The "mud-flat" pattern closely resembles that found on glass surfaces after sodium exchange treatments [14–16]. At even higher ion doses the "island" regions between the cracks began to flake off, leaving copious debris on the glass surface. It is apparent that the zero effective toughness condition alluded to in our earlier discussion of Equation 4 has been attained in the proton irradiation experiments.

We are now in a position to correlate the

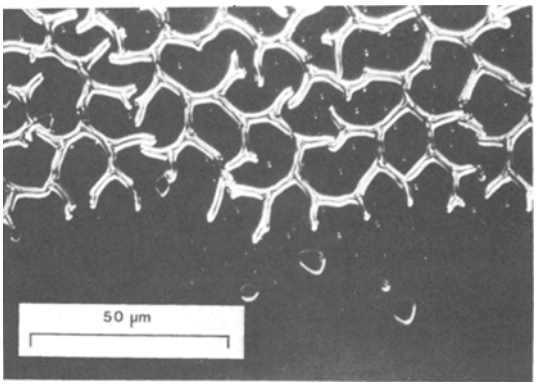

Figure 3 Optical micrograph of soda-lime glass surface irradiated with 480 kV protons at dose 2×10^{20} ions m^{-2}. (Lower region was masked from incident beam.) "Mud-flat" pattern is due to intersection of spontaneously propagated, shallow surface cracks.

experimental data in Fig. 2 with the indentation theory of Section 2. Taking note of Eernisse's observation that surface stress, σ_s, increases linearly with radiation dose, D, in the sub-saturation region, we may conveniently write

$$D/D_c = 2\psi\sigma_s d^{1/2}/K_c \quad (6)$$

so that Equation 5 transforms to

$$c/c_0 = 1/(1 - D/D_c)^{2/3} \quad (7)$$

Note that $c = c_0$ at $D = 0$, as required; also that $c \to \infty$ at $D = D_c$, so D_c is the critical dose for spontaneous cracking. Taking $c_0 = 63\,\mu m$ and $D_c = 2.5 \times 10^{19}$ protons m^{-2}, we generate from Equation 7 the solid curve shown in Fig. 2. This curve passes through the data points up to the dose level at which surface crazing first becomes apparent. Using $\psi = 1$ (see Appendix), $K_c = 0.75$ MPa $m^{1/2}$ for soda-lime glass [17], we may evalute Equation 6 at $D = D_c$ to obtain $\sigma_s d^{1/2} = 0.38$ MPa $m^{1/2}$ at the saturation point. For $d = 5\,\mu m$ this yields $\sigma_s = 168$ MPa, which is in the strength range of as-received glass surfaces (typically 100 to 200 MPa [18, 19]). In terms of an equivalent surface line force, we have $\sigma_s d = 840$ N m^{-1}, to be compared with Eernisse's value of 500 N m^{-1}.

4. Discussion

We have developed a formulation for evaluating surface layer stresses from indentation crack measurements. The method is simple in principle, requiring only access to a standard hardness testing facility. By means of our illustrative case study on proton-irradiated glass, we have been able to demonstrate the capacity of the method for predicting quantitative trends, if not accurate absolute values. *En route* to this experimental confirmation of the fracture mechanics equations we have found an explanation for the limiting stress capacity of ion-bombarded surfaces, namely surface crazing, which could have some bearing on the erosion and wear properties of ion-implanted materials [20]. We have also established a stress intensity factor formalism, via Equations 1 and 2, suitable for analysing the role of residual stress effects (associated with both flaw generation and surface stress state) in the determination of strength characteristics [21]. This latter is an area which we shall explore in greater detail elsewhere, particularly in relation to machining damage in ceramics [22].

In proposing the indentation technique as a surface stress probe, we need to point out some of the potential experimental complications that might arise. First and foremost, the material system under investigation must be "well-behaved" insofar as the indentation fracture pattern is concerned. Specimens with insufficiently smooth surfaces or with coarse microstructures (relative to the scale of the indentation itself) may not produce measurable radial crack traces [8]. Choice of indentation load is also important: the load should not be too small that the radial traces remain too close to the elastic/plastic zone (typically, the radial tips should extend at least twice the distance from the contact centre as the corner of the hardness impression, in order that Equation 1 remain valid); nor should it be too large that chipping occurs due to excessive growth of lateral cracks (possibly enhanced by any tendency for the surface stressing process to cause delamination of the type mentioned in Section 3). Again, since our theoretical model is based on the concept of equilibrium fracture some effort should strictly be made to exclude from the test environment any "reactive" chemical species, most notably water, which can promote subcritical extension in the post-indentation configuration [8]. The simplest practical way of achieving an effective inert environment is to direct a stream of dry nitrogen gas onto the specimen surface throughout the entire indentation test procedure, measuring the crack traces as soon as possible (preferably within 1 min) after completion of the contact cycle.

It is also important that we should not lose sight of the assumptions made in constructing the theoretical model. We have mentioned that the introduction of a surface stress layer will tend to distort the penny-like geometry of the radial cracks, particularly when the intensity of stress is high and the layer is thin. Under such circumstances we may expect the subsurface crack regions to constrain the expansion or contraction of the radial traces, thereby leading to underestimates in the stress evaluations. However, the fact that our estimates for ion-irradiated glass were actually in excess of those by Eernisse in comparable experiments suggests that the constraining effect may not be great. Again, Equation 2 is derived in the approximation $d \ll c$, and there may be instances were this proviso breaks down. If so, Equation 2 needs to be replaced by a more general formula; this generalization must incorporate a crack-size dependence, since at $d = c$ the stress intensity factor must reduce to the familiar solution for uniformly stressed cracks, $K_s \propto \sigma_s c^{1/2}$. Reference is made to the Appendix for the derivation of such a formula, which can be used to obtain a modified (somewhat more complicated) equivalent of Equation 5 for stress evaluation. A further possible complication is that the stress field is not uniform within the surface layer, but rather exhibits a gradient with depth. The necessary formalism for accommodating this effect is also included in the Appendix. What our existing expressions give us, of course, is the *average* stress over the surface layer.

Finally, in using indentation crack size to monitor trends in surface stress behaviour, as we have done in Fig. 2, it is as well to appreciate that d, as well as σ_s, may vary with time. With the proton-irradiated glass considered here the penetration depth is fixed by the incident energy of the ions, so the crack size uniquely reflects the magnitude of the surface stress. In processes such as chemical tempering by ion exchange in molten salts, however, the depth profile changes significantly with duration of treatment [23]. Clearly in such cases an independent experiment would be required to separate out the relative contributions from the σ_s and d variations to the crack-size dependence in Equation 5.

Acknowledgements

The results discussed in Section 3 were obtained by T. Jensen as part of an honours thesis program at the School of Physics, The University of New South Wales. Funding for the remainder of this work was provided by the U.S. Office of Naval Research, Metallurgy and Ceramics Program.

Appendix

Here we give details of the calculation from which Equation 2 derives. Our starting point is the solution for the stress intensity factor at the periphery of an embedded penny crack of radius c acted upon by an internal, concentrated point force. The specific configuration we shall consider is shown in Fig. A1. Writing $\sigma_s(x, y)\,dx\,dy$ as the point force, we seek an integrated solution over the shaded strip areas defined by width d and depth b to obtain the stress intensity factor K_s at the symmetry point S. Then for $b = 0$, this integrated solution may be taken as representative of the *half*-penny radial crack system of Fig. 1, provided due allowance is made for free-surface and crack interaction (radial–radial and radial–lateral) effects.

Accordingly, our incremental stress intensity factor, from [9], is

$$dK_s(x, y) = [\psi\sigma_s(x, y)/2\pi c^{1/2}]\{(c^2 - x^2 - y^2)^{1/2}/[(c - x)^2 + y^2]\}\,dx\,dy \qquad (A1)$$

where ψ is a dimensionless term which incorporates the necessary free-surface and crack-interaction corrections. This ψ term is here defined to be consistent with familiar limiting solutions (see

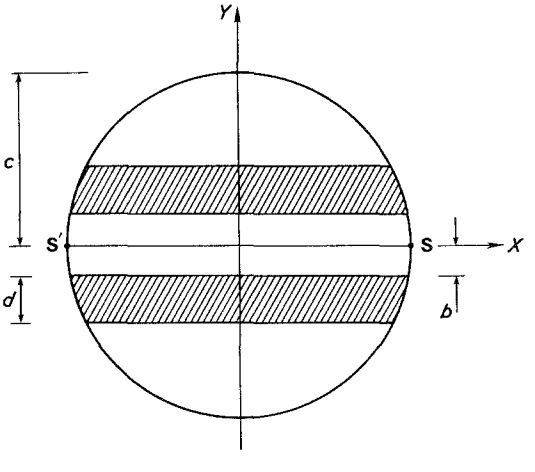

Figure A1 Embedded penny crack subjected to stresses over mirror-symmetric strip areas (shaded). Stress intensity factor solution is equivalent to that for half-penny configuration with surface trace SS', provided free-surface and crack-interaction correction factors are included.

Equation A12, below); for indentation systems it should not differ too greatly from the exact value $2/\pi^{1/2}$ for the embedded penny crack of Fig. A1 [9]. The requisite integral over the shaded areas of Fig. 1 is

$$K_s = 2\int_b^{b+d} \int_{-(c^2-y^2)^{1/2}}^{+(c^2-y^2)^{1/2}} dK_s(x,y) \quad (A2)$$

(Here the factor 2 is to take care of the mirror symmetry about the x axis.) For the special case $\sigma_s = \text{const.}$, Equations A1 and A2 combine to give

$$K_s = (\psi\sigma_s/\pi c^{1/2})\int_b^{b+d} L(y)\,dy \quad (A3)$$

where we define the integral

$$L(y) = \int_{-(c^2-y^2)^{1/2}}^{+(c^2-y^2)^{1/2}} \{(c^2-x^2-y^2)^{1/2}/[(c-x)^2+y^2]\}\,dx \quad (A4)$$

To solve Equation A4 we consider the following contour integral [24]:

$$I = \oint_C \{(c^2-z^2-y^2)^{1/2}/[(c-z)^2+y^2]\}\,dz \quad (A5)$$

where z is a vector in complex space. The integrand in Equation A5 has a branch cut between the branch points $z = \pm(c^2-y^2)^{1/2}$, so we choose the contour $C = C_0 + C_1 + C_2 + C_3 + C_4 + C_5$ shown in Fig. A2. Evaluations over each segment of the contour give

$$\int_{C_0} = 0 \quad (A6a)$$

$$\int_{C_1} = \int_{C_5} = -L \quad (A6b)$$

$$\int_{C_2} = -\int_{C_4} \quad (A6c)$$

$$\int_{C_3} = -2\pi \quad (A6d)$$

(The minus sign in Equation A6b arises from proper consideration of the phase of the integrand above and below the branch cut [24].) Hence the integrals in Equations A4 and A5 are related according to

$$I = -2(L+\pi) \quad (A7)$$

Now by the residue theorem [24] the integral I is also given by $2\pi i$ times the sum of the residues at the poles. The integrand in Equation A5 has simple

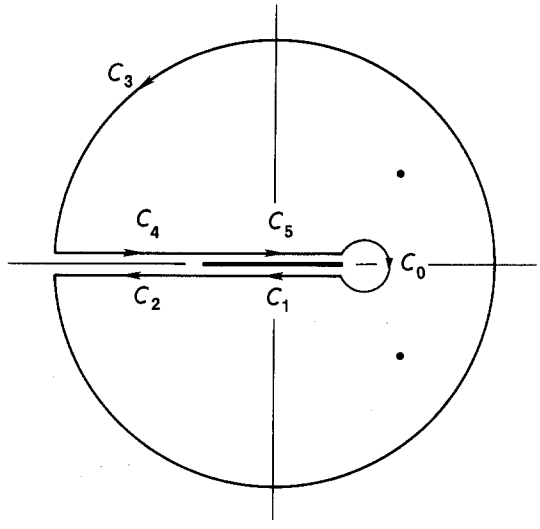

Figure A2 Contour in complex space for evaluating integral I. The function to be integrated has branch cut (heavy line) between $z = \pm(c^2-y^2)^{1/2}$ and simple poles at $z = c \pm iy$ (heavy dots). The contour C is subdivided into circular segments C_0 and C_3, linear segments C_1 and C_5 adjacent to the branch cut, and linear segments C_2 and C_4 to complete the circuit.

poles at $z = c \pm iy$. Computation of the residues for these poles leads to the result

$$I = -2\pi(c/y)^{1/2} \quad (A8)$$

Combining Equations A7 and A8, we obtain

$$L(y) = \pi[(c/y)^{1/2} - 1] \quad (A9)$$

On substituting Equation A9 back into Equation A3 and completing the remaining straightforward integration, we get

$$K_s = \psi\sigma_s c^{1/2}[2(b/c + d/c)^{1/2} - 2(b/c)^{1/2} - d/c] \quad (A10)$$

For a stress layer located at the surface our solution reduces to

$$K_s(b=0) = \psi\sigma_s d^{1/2}[2 - (d/c)^{1/2}] \quad (A11)$$

Note that for a strip which extends to the depth of the crack Equation A11 in turn reduces to

$$K_s(b=0, d=c) = \psi\sigma_s c^{1/2} \quad (A12)$$

which is the familiar result for a uniform stress field. It is this last expression which provides us with a reference base for defining and calibrating a convenient crack geometry factor for our half-penny radial crack system. Thus, actual strength measurements of glass specimens containing Vickers indentations [25, 26] can be shown to be

consistent with a value unity for ψ (to within an experimental uncertainty of about ± 10%; cf. the value $2/\pi^{1/2}$ for ideal embedded pennies). The *particular* solution of interest here is the limiting case of Equation A11 for thin layers,

$$K_s(b = 0, d \ll c) = 2\psi\sigma_s d^{1/2} \qquad \text{(A13)}$$

corresponding to Equation 2 in the main text.

We may note in passing that the general solution for *non-uniform* depth profiles could be derived in much the same way as above, but incorporating $\sigma_s(y)$ *within* the integral of Equation A3; i.e. in conjunction with Equation A9,

$$K_s = (\psi/c^{1/2}) \int_b^{b+d} [(c/y)^{1/2} - 1]\sigma_s(y)\, dy \qquad \text{(A14)}$$

References

1. T. JENSEN, B. R. LAWN, R. L. DALGLISH and J. C. KELLY, *Radiat. Eff.* **28** (1976) 245.
2. D. B. MARSHALL and B. R. LAWN, in Proceedings of the 7th Australian Ceramic Conference (Australian Ceramic Society, Sydney, 1976).
3. *Idem, J. Amer. Ceram. Soc.* **60** (1977) 86.
4. B. R. LAWN and M. V. SWAIN, *J. Mater. Sci.* **10** (1975) 113.
5. D. B. MARSHALL and B. R. LAWN, *ibid.* **14** (1979) 2001.
6. B. R. LAWN, D. B. MARSHALL and A. G. EVANS, *J. Amer. Ceram. Soc.* **63** (1980) 574.
7. D. B. MARSHALL, B. R. LAWN and A. G. EVANS, *ibid.* **65** (1982) 561.
8. G. R. ANSTIS, P. CHANTIKUL, D. B. MARSHALL and B. R. LAWN, *ibid.* **64** (1981) 533.
9. H. TADA, P. C. PARIS and G. R. IRWIN, "The Stress Analysis of Cracks Handbook" (Dell Research Corp., Hellertown, PA, 1973) p. 24.2.
10. T. JENSEN, Honours Program thesis, School of Physics, University of New South Wales (1975).
11. E. P. EERNISSE, *J. Appl. Phys.* **45** (1974) 167.
12. A. A. GRIFFITH, *Phil. Trans. Roy. Soc. (Lond.)* **A221** (1920) 163.
13. B. R. LAWN and T. R. WILSHAW, "Fracture of Brittle Solids" (Cambridge University Press, London, 1975) Chap. 2.
14. E. N. ANDRADE and L. C. TSIEN, *Proc. Roy. Soc. (Lond.)* **A159** (1937) 346.
15. J. E. GORDON, D. M. MARSH and M. E. PARRATT, *ibid.* **A249** (1959) 65.
16. F. M. ERNSBERGER, *ibid.* **A257** (1960) 213.
17. S. M. WIEDERHORN, *J. Amer. Ceram. Soc.* **52** (1969) 99.
18. R. E. MOULD, in "Fundamental Phenomena in the Materials Sciences", Vol. 4, edited by L. J. Bonis, J. J. Duga and J. J. Gilman (Plenum Press, New York, 1967) p. 119.
19. B. R. LAWN, D. B. MARSHALL, P. CHANTIKUL and G. R. ANSTIS, *J. Aust. Ceram. Soc.* **16** (1980) 4.
20. M. G. S. NAYLOR and T. F. PAGE, *J. Microsc.* **130** (1983) 345.
21. D. B. MARSHALL, B. R. LAWN and P. CHANTIKUL, *J. Mater. Sci.* **14** (1979) 2225.
22. B. R. LAWN, E. R. FULLER, D. B. MARSHALL and R. F. COOK, to be published.
23. J. S. OLCOTT, *Science* **140** (1963) 1189.
24. J. MATHEWS and R. L. WALKER, "Mathematical Methods of Physics" (W. A. Benjamin, Inc., New York, 1964).
25. D. B. MARSHALL and B. R. LAWN, *J. Amer. Ceram. Soc.* **63** (1980) 532.
26. R. F. COOK and B. R. LAWN, *ibid.* **66** (1983) C-200.

Received 6 February
and accepted 29 February 1984